

Effect of RANS Model on the Aerodynamic Characteristics of a Train in Crosswinds Using DDES

Tian Li^{1,*}, Zhiyuan Dai¹ and Weihua Zhang¹

Abstract: Detached eddy simulation has been widely applied to simulate the flow around trains in recent years. The Reynolds-averaged Navier-Stokes (RANS) model for delayed detached eddy simulation (DDES) is an essential user input. The effect of the RANS model for DDES on the aerodynamic characteristics of a train in crosswinds is investigated in this study. Three different DDES models are used, based on the Spalart-Allmaras model (SA), the realizable $k-\varepsilon$ model (RKE), and the shear stress transport $k-\omega$ model (SST). Results show that all DDES models can give relatively accurate predictions of pressure coefficient on almost all surfaces. There are only some specific differences in the small vortices, while similar flow patterns around trains could be predicted. The SST based DDES model (SSTDDES) gives the most accurate numerical results among the three models for the surface pressure. The variations in pressure on the leeward face play a key role in the variation of the side force.

Keywords: Numerical simulation, DES, train aerodynamics, crosswind, RANS.

1 Introduction

Numerical simulation has been a valid tool to study train aerodynamics in recent years [Baker (2019)]. Due to the low cost, computational fluid dynamic (CFD) simulation has become more popular with the fast development of the high performance computational resources [Li, Zhang, Rashidi et al. (2019)].

RANS has been widely applied to simulate the flow around trains due to the low cost and high calculation efficiency. According to the study by Li et al. [Li, Zhang, Rashidi et al. (2019); Li, Qin and Zhang (2019); Yu, Jiang, Zhang et al. (2019); Morden, Hemida and Baker (2015); Wang, Bell, Burton et al. (2017)], RANS is able to predict the surface pressure and aerodynamic forces of a train accurately. Numerical simulation using the SST $k-\omega$ model together with a second order discretization scheme provides the closest results to the experimental surface pressure for a so-called ideal train with a simplified geometry [Li, Zhang, Rashidi et al. (2019)]. By comparison with other models, Li et al. [Li, Qin, Li et al. (2019); Li, Hemida, Zhang et al. (2018)] found that the SST $k-\omega$ model could accurately predict aerodynamic forces. Wang et al. [Wang, Bell, Burton et al. (2017)] evaluated the accuracy of unsteady RANS applied to the prediction of slipstreams.

¹ State-Key Laboratory of Traction Power, Southwest Jiaotong University, Chengdu, 610031, China.

* Corresponding Author: Tian Li. Email: litian2008@home.swjtu.edu.cn.

Received: 27 July 2019; Accepted: 21 November 2019.

Wilson et al. [Wilson, Stern, Coleman et al. (2001)] studied the hydrodynamic characteristic of ships by means of RANS. Walters et al. [Walters and Cokljat (2008)] established a three-equation eddy-viscosity model for RANS, and the test cases proved the ability of the model to reproduce transitional flow characteristics with a legitimate degree of accuracy. Although RANS is widely used, it has a weakness in predicting the flow around trains in both time and space.

Detached eddy simulation (DES) combines the advantages of both RANS and large eddy simulation (LES). The RANS model is used to predict the flow near the solid boundaries, and the LES model is adopted to simulate domains far from the wall [Hemida and Krajnovic (2009)]. DES has been applied for the numerical simulation of unsteady flow issues in recent years [Bangga, Weihing, Lutz et al. (2017); Chen and Li (2019)]. Hedges et al. [Hedges, Travin and Spalart (2002)] calculated the flow around a generic airliner landing-gear truck using the DES. Chen et al. [Chen, Gao and Zhu (2016)] investigated the flows around a high-speed train through the DES. Li et al. [Li, Hemida, Zhang et al. (2018)] and Morden et al. [Morden, Hemida and Baker (2015)] conducted comparisons in surface pressure between the wind-tunnel data and numerical results obtained using the DES. Flynn et al. [Flynn, Hemida, Soper et al. (2014)] investigated the highly non-stationary slipstreams of a Class 66 train using the DDES. Xia et al. [Xia, Wang, Shan et al. (2017)] studied the effects of ground configurations on the slipstream of trains with the improved delayed detached eddy simulation (IDDES). The aerodynamic characteristics of trains with double units or a single unit were studied by Guo et al. [Guo, Liu, Yu et al. (2019)]. The IDDES approach was used to obtain the aerodynamic coefficients, the time-averaged and instantaneous flow. The IDDES approach was also used to simulate the unsteady aerodynamic forces by Niu et al. [Niu, Wang, Zhang et al. (2018)]. The assessment of several turbulence modelling approaches including the Embedded large eddy simulation, Scale-adaptive simulation, and RANS was conducted by Maleki et al. [Maleki, Burton and Thompson (2017)]. It was found that the results obtained using the ELES and SAS agreed with the wind tunnel data. The steady RANS model failed to predict the aerodynamic forces. In either DES or DDES, RANS is applied to solve the flow field in the near-wall regions. Therefore, the DDES model is based on one of the RANS models, including the SA, RKE and SST. According to the authors' knowledge, there is little research on the effect the RANS model for the DDES on the aerodynamic characteristics of trains. In this paper, the effect of the RANS model for the DDES on the aerodynamic characteristics of a train in crosswinds is investigated. The numerical results are compared with the experimental ones.

2 RANS based DDES models

The RANS equations are time-averaged ones of the motion of fluid or flow. The fundamental idea for the derivation is Reynolds decomposition, in which the instantaneous variables can be divided into the time-averaged component and the fluctuating component. With the turbulence models developed for the Reynolds stress, which is a crucial variable for the closure problem, the RANS equations can be solved using CFD. Three typical RANS models are SA, RKE and SST.

DES is an improvement of the RANS model, which combines the advantages of both RANS and LES. If the turbulent length scale \tilde{d} is less than $C_{DES}\Delta_{\max}$, the RANS model

is adopted in those regions, and the other regions are assigned the LES mode. Where Δ_{\max} is the largest side of the computational cell, and the empirical constant C_{DES} has a value of 0.65.

2.1 SA based DDES model (SADDES)

The SA model contains one transport equation for kinematic eddy viscosity parameter $\tilde{\nu}$ and a specification of a length scale d , which allows the economical computation of boundary layers in aerodynamics.

The equation of the turbulent variable $\tilde{\nu}$ in the SA model [Vatsa, Lockard and Spalart (2017)] is written as

$$\frac{\partial \tilde{\nu}}{\partial t} + u_j \frac{\partial \tilde{\nu}}{\partial x_j} = c_{b1}(1 - f_{t2})\tilde{S}\tilde{\nu} - \left(c_{\omega 1} f_{\omega} - \frac{c_{b1}}{\kappa^2} \right) \left(\frac{\tilde{\nu}}{d} \right)^2 + \frac{1}{\sigma} \left\{ \frac{\partial}{\partial x_j} \left[(\nu + \tilde{\nu}) \frac{\partial \tilde{\nu}}{\partial x_j} \right] + c_{b2} \frac{\partial \tilde{\nu}}{\partial x_i} \frac{\partial \tilde{\nu}}{\partial x_i} \right\} + f_{t1} \Delta U^2, \quad (1)$$

in which

$$\begin{aligned} \mu_t &= \rho \tilde{\nu} f_{v1}, \quad \chi = \frac{\tilde{\nu}}{\nu}, \quad \tilde{S} = \Omega + \hat{s}, \quad \hat{s} = \frac{\tilde{\nu}}{\kappa^2 d^2} f_{v2}, \quad f_{v1} = \frac{\chi^3}{\chi^3 + c_{v1}^3}, \quad f_{v2} = 1 - \frac{\chi}{1 + \chi f_{v1}}, \\ f_{\omega} &= g \left(\frac{1 + c_{\omega 3}^6}{g^6 + c_{\omega 3}^6} \right)^{\frac{1}{6}}, \quad g = r + c_{\omega 2}(r^6 - r), \quad r = \min \left(\frac{\tilde{\nu}}{\tilde{S} \kappa^2 d^2}, 10 \right), \quad f_{t2} = c_{t3} \exp(-c_{t4} \chi^4), \\ f_{t1} &= c_{t1} g_t \exp \left(-c_{t2} \frac{\omega_t^2}{\Delta U^2} (d^2 + g_t^2 d_t^2) \right), \quad g_t = \min \left[0.1, \frac{\Delta U}{\omega_t \Delta x_t} \right], \end{aligned}$$

where ρ is the density, $\nu = \frac{\mu}{\rho}$ is the kinematic viscosity, μ is the molecular dynamic viscosity, Ω is the magnitude of the vorticity, ΔU is the difference of velocity between the field point and the wall, Δx_t is the grid spacing, ω_t is the wall vorticity, d_t is the distance between the field point and the wall. Constants are defined as, $c_{t1} = 1$, $c_{t2} = 2$, $c_{b1} = 0.1355$, $c_{b2} = 0.622$, $\sigma = 2/3$, $\kappa = 0.41$, $c_{\omega 1} = \frac{c_{b1}}{\kappa^2} + \frac{1 + c_{b2}}{\sigma}$, $c_{\omega 2} = 0.3$, $c_{\omega 3} = 2$, $c_{v1} = 7.1$, $c_{t3} = 1.2$, $c_{t4} = 0.5$.

In the SA model, the length scale d , which is defined by the shortest distance to the wall, determines partly the destruction of the turbulent viscosity and level of production. The SADES model [Shur, Spalart, Strelets et al. (1999)] uses a new length scale \tilde{d} instead of d . The new length scale is defined as

$$\tilde{d} = \min(d, C_{DES} \Delta_{\max}), \quad (2)$$

Eq. (2) ensures the RANS model is applied in the entire boundary layer in the case that Δ_{\max} is smaller than the size of the boundary layer.

In the SADDES, the length scale \tilde{d} is redefined by

$$\tilde{d} = d - f_d \max(0, d - C_{DES} \Delta_{\max}), \quad (3)$$

where $f_d = 1 - \tanh([8r_d]^3)$ and $r_d = \frac{v_t + \nu}{\sqrt{U_{i,j}U_{i,j}} \kappa^2 d^2}$.

2.2 RKE based DDES model (RKEDES)

The RKE model is an improvement over the standard k - ε model. It provides the better predictions for flows involving separation and recirculation.

In the RKE model, the equation [Tian and Lu (2013)] for turbulent kinetic energy k is

$$\frac{\partial(\rho k)}{\partial t} + \frac{\partial(\rho u_i k)}{\partial x_i} = \frac{\partial}{\partial x_i} \left[\left(\mu + \frac{\mu_t}{\sigma_k} \right) \frac{\partial k}{\partial x_i} \right] - \rho \varepsilon + Y_k \quad (4)$$

The equation for turbulent dissipation ε is

$$\frac{\partial(\rho \varepsilon)}{\partial t} + \frac{\partial(\rho u_i \varepsilon)}{\partial x_i} = \frac{\partial}{\partial x_i} \left[\left(\mu + \frac{\mu_t}{\sigma_\varepsilon} \right) \frac{\partial \varepsilon}{\partial x_i} \right] + \rho C_{1S} \varepsilon - \rho C_{2\varepsilon} \frac{\varepsilon^2}{k + \sqrt{\nu \varepsilon}} \quad (5)$$

in which

$$\mu_t = \rho C_\mu \frac{k^2}{\varepsilon}, \quad C_1 = \max \left\{ 0.43, \frac{kS}{kS + 5\varepsilon} \right\}, \quad S = \sqrt{2S_{ij}S_{ij}}, \quad C_\mu = \frac{\varepsilon}{A_0 \varepsilon + A_s k \sqrt{S_{ij}S_{ij} + \tilde{\Omega}_{ij}\tilde{\Omega}_{ij}}},$$

$$\tilde{\Omega}_{ij} = \bar{\Omega}_{ij} - 3\varepsilon_{ijk}\omega_k.$$

where S is the modulus of the mean rate-of-strain tensor, $\bar{\Omega}_{ij}$ is the mean rate-of-rotation tensor. The constants are given by $C_{2\varepsilon} = 1.9$, $\sigma_k = 1.0$, $\sigma_\varepsilon = 1.2$, $A_0 = 4.04$,

$$A_s = \sqrt{6} \cos\left(\frac{1}{3} \cos^{-1}(\sqrt{6}W)\right), \quad W = \frac{S_{ij}S_{jk}S_{ki}}{\tilde{S}^3}, \quad \tilde{S} = \sqrt{S_{ij}S_{ij}}.$$

In the DES model based on RKE (RKEDES), the dissipation term in the RKE model Y_k is modified as

$$Y_k = \frac{\rho k^{3/2}}{\tilde{d}}, \quad (6)$$

and

$$\tilde{d} = \min\left(\frac{k^{3/2}}{\varepsilon}, C_{DES} \Delta_{\max}\right), \quad (7)$$

The delayed option can also be applied to the RKEDES model to prevent the activation of LES model throughout the boundary layer. The length \tilde{d} in Eq. (6) is redefined as

$$\tilde{d} = \frac{k^{3/2}}{\varepsilon} - f_d \max\left(0, \frac{k^{3/2}}{\varepsilon} - C_{DES} \Delta_{\max}\right), \quad (8)$$

The formulation f_d is similar to the Eq. (3) for SADDDES.

2.3 SST based DDES model (SSTDDES)

The SST model was developed based on the standard k - ω model to improve the separation prediction in the near-wall region by Menter [Menter (1994)]. The equation for turbulent kinetic energy k is

$$\frac{\partial \rho k}{\partial t} + \frac{\partial \rho U_i k}{\partial x_i} = \frac{\partial}{\partial x_i} \left[(\mu + \sigma_k \mu_t) \frac{\partial k}{\partial x_i} \right] + Y_k - \beta^* \rho k \omega. \quad (9)$$

The equation for turbulent dissipation ω is

$$\frac{\partial \rho \omega}{\partial t} + \frac{\partial \rho U_i \omega}{\partial x_i} = \frac{\partial}{\partial x_i} \left[(\mu + \sigma_\omega \mu_t) \frac{\partial \omega}{\partial x_i} \right] + 2(1 - F_1) \rho \omega^2 \frac{1}{\omega} \frac{\partial k}{\partial x_i} \frac{\partial \omega}{\partial x_i} + \alpha \rho S^2 - \beta \rho \omega^2 \quad (10)$$

in which

$$F_1 = \left\{ \left\{ \min \left[\max \left(\frac{\sqrt{k}}{\beta^* \omega y}, \frac{500\nu}{y^2 \omega} \right), \frac{4\rho\sigma_{\omega 2} k}{CD_{k\omega} y^2} \right] \right\}^4 \right\}, \quad CD_{k\omega} = \max \left(2\rho\sigma_{\omega 2} \frac{1}{\omega} \frac{\partial k}{\partial x_i} \frac{\partial \omega}{\partial x_i}, 10 \right)$$

$$\mu_t = \frac{\alpha_1 k}{\max(\alpha_1 \omega, SF_2)}, \quad F_2 = \tanh \left\{ \left[\max \left(\frac{\sqrt{k}}{\beta^* \omega y}, \frac{500\nu}{y^2 \omega} \right) \right]^2 \right\}.$$

where ρ is the density, μ is the molecular dynamic viscosity, S is the invariant measure of the strain rate. The constants are calculated by a blend from the corresponding constants via $\alpha = \alpha_1 F + \alpha_2 (1 - F)$. Constants are $\beta^* = 0.09$, $\alpha_1 = 5/9$, $\beta_1 = 3/40$, $\sigma_{k1} = 0.85$, $\alpha_2 = 0.44$, $\beta_2 = 0.0828$, $\sigma_{k2} = 1$, $\sigma_{\omega 2} = 0.856$

In the DES model based on the SST, the dissipation term of the turbulent kinetic energy Y_k in the SST turbulence model [Menter, Kuntz and Langtry (2003)] is modified as

$$Y_k = \rho \beta^* k \omega F_{DES}, \quad (11)$$

$$F_{DES} = \max \left(\frac{L_t}{C'_{DES} \Delta_{\max}}, 1 \right), \quad (12)$$

and

$$L_t = \frac{\sqrt{k}}{\beta^* \omega}, \quad (13)$$

where the empirical constant C'_{DES} has a value of 0.61. Similarly, the delayed option can also be used to ensure the proper application throughout the boundary layer. The F_{DES} in Eq. (11) is modified as

$$F_{DES} = \max\left(\frac{L_t}{C'_{DES}\Delta_{\max}}(1 - F_{SST}), 1\right), \quad (14)$$

F_{SST} can be selected from 0, F_1 or F_2 . Herein, F_1 and F_2 are the blending functions in the SST. The chosen of F_{SST} is introduced in detail by Mentor et al. [Menter, Kuntz and Langtry (2003)].

3 Numerical information

Since there were several experimental results [Hemida and Krajnović (2009)] reported for the ICE2 (Inter-city Express) train, the 1/8th scaled train model was chosen in this investigation. Similar to the train model used in the experiments, the numerical geometry of the train consists of a leading car and a half trailer car, which is shown in Fig. 1. The leading car has a length of 2.6585 m, a width of 0.302 m and a height of 0.4117 m. In this study, the characteristic length H is defined by the train height. Based on the characteristic length, the Reynolds number is about 1.9×10^6 . Therefore, the flow around the train is fully turbulent.

Several pressure taps are located at 6 different loops, which are $x = -0.11, -0.25, -0.5, -1.57, -2.06$ and -2.49 m, respectively.

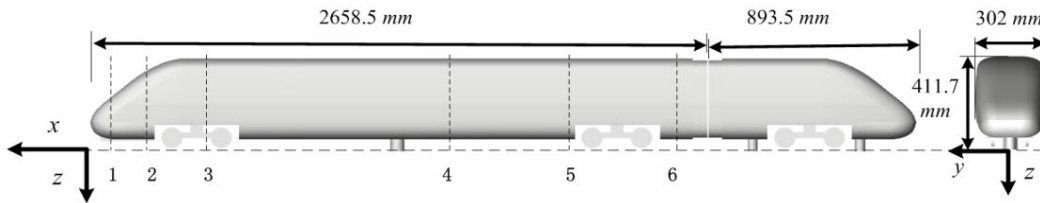


Figure 1: Train model

The computational domain is similar to that used by Li et al. [Li, Qin, Li et al. (2019); Morden, Hemida and Baker (2015)]. It is $40H$ in length, $26H$ in width, and $10H$ in height. The nose tip is $12H$ far from the inlet boundaries, and the train tail is $20H$ far from the outlet boundaries. The boundary conditions are consistent with those used by Li et al. [Li, Qin and Zhang (2019); Morden, Hemida and Baker (2015)].

The entire computational domain is discretized with unstructured hexahedral grids. In the computational domain, there are four refinement boxes around the train to ensure a high resolution. A boundary layer mesh is added close to the train surface and ground, which makes the non-dimensional parameter y^+ around 1. Fig. 2 shows the mesh on the cross-section $y=0$.

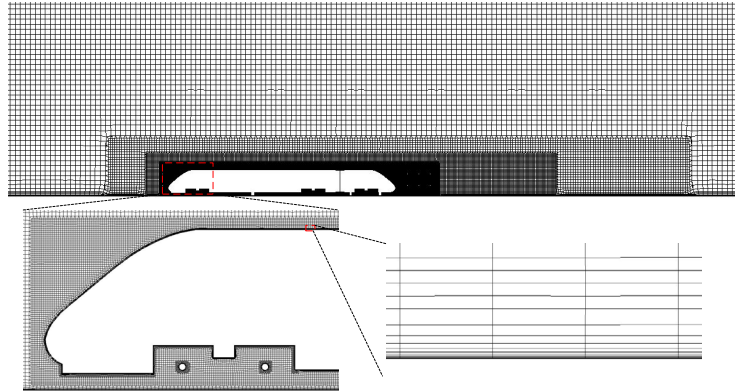


Figure 2: Mesh on the cross-section $y=0$ m

Numerical simulations are carried out using the commercial CFD software Ansys Fluent. The Semi Implicit Method for Pressure Linked Equation Consistent (SIMPLEC) is used for the pressure-velocity coupling. The time step for the DDES is $\Delta t=2.0 \times 10^{-5}$ s. The second-order upwind scheme is chosen for the discretization of all variables.

4 Results

In the following, the effect of the RANS model on the flow around the train in crosswinds is investigated. The flow around the train is discussed in terms of the time-averaged surface pressure, time-averaged skin friction, time-averaged flow field, unsteady aerodynamic forces and instantaneous surface pressure.

4.1 Time-averaged surface pressure

The time-averaged pressure coefficient c_p at different loops along the length of the train body is shown in Fig. 3. The circular symbols in Fig. 3 represent the experimental data [Hemida and Krajnović (2009)]. Three different turbulent models are the SADDES, RKEDDES and SSTDES, respectively. It can be observed that all numerical simulations give relatively accurate predictions for the pressure coefficient on almost all surfaces due to the relatively small differences between numerical and experimental results.

The highest pressure is found at the corner of the roof and leeward face at the loop $x_2=-0.25$ m, and the maximum suction pressure is found on the windward face of the streamlined nose at the loop $x_1=-0.11$ m. Meanwhile, the pressure distribution on the non-streamline train body is similar at difference loops. On the windward face, the pressure is mainly positive, whereas the pressure is almost negative on the top, bottom and leeward face.

The pressure predicted by all approaches is almost consistent on the windward face, which corresponds to the angle between 225° and 315° . The RANS models in the DDES give specific differences in the pressure on the bottom and slight differences in pressure on the leeward face. The SADDES gives a close agreement in the pressure on the bottom at $x_1=-0.11$ m and $x_2=-0.25$ m. Compared to the SADDES and RKEDDES models, the SSTDES predicts a closer fit in the maximum suction pressure.

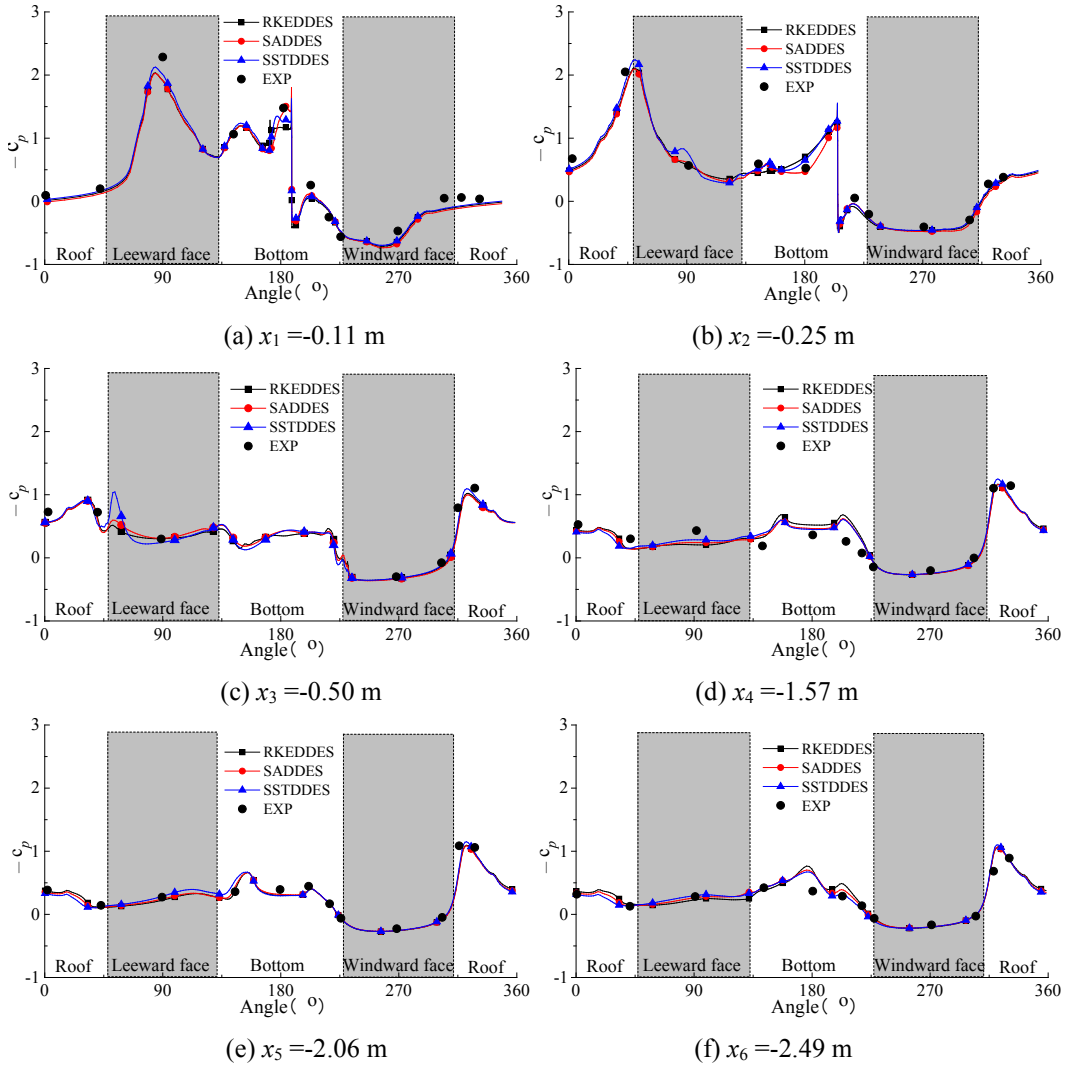


Figure 3: Pressure distribution at different loops obtained using different approaches

4.2 Time-averaged skin friction

Skin friction forces are caused by the viscosity of airflow, which is a component of the aerodynamic forces. The time-averaged skin friction coefficient is a dimensionless wall shear stress.

The mean skin friction coefficient c_f obtained at different loops is shown in Fig. 4 by means of different DDES approaches. Two loops are located at $x_2 = -0.25$ m and $x_3 = -0.50$ m. In general, the skin friction on the streamline nose is larger than that on the train body. The maximum skin friction coefficient is found at the corner of roof and leeward face at the loop $x_2 = 0.25$ m. It can be observed that all numerical simulations show considerable difference in the skin friction coefficient at all corners. In the streamline nose, SADDDES

predicts the largest value at almost all corners.

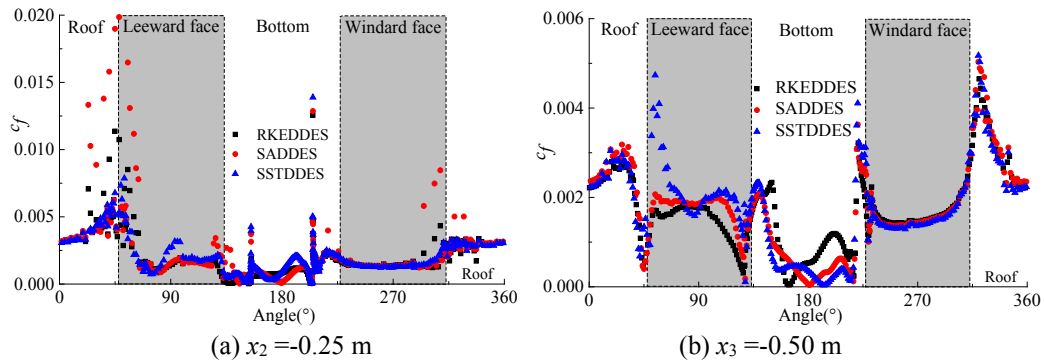
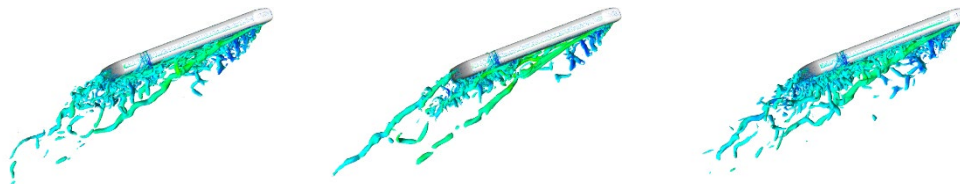


Figure 4: Mean skin friction coefficient at different loops

4.3 Time-averaged flow field

Iso-surfaces of the second invariant of the time-averaged velocity gradient can be visualized to investigate the flow field around the train. Fig. 5 shows the comparison of the iso-surfaces of the second invariant of the time-averaged velocity gradient at two different levels for the three different approaches. The level l represents the ratio between the local second invariant of the time-averaged velocity gradient and the maximum one. All DDES approaches give similar primary vortices in the wake flow. It can be seen from Figs. 5(a)-5(c) that the primary vortex separated from the train nose is almost parallel to the one separated from the train tail. The angles of those primary vortices are nearly 30° , which corresponds to the yaw angle of the incoming flow. Meanwhile, there are vortices separated from the first bogie. The magnitude of the vortices separated from the train body is smaller than that of the above primary vortices.

It is found that there are certain differences in the small vortices obtained using different DDES models. The RKEDDES predicts fewer vortices in the wake flow than the SADDES and SSTDDDES do. Meanwhile, the vortex shells obtained using the SADDES are quite similar to those for the SSTDDDES. In general, both the SST and SA models give a more accurate flow field around the train due to the demand for high-quality meshes in the boundary layer for RANS. Therefore, the vortices in the boundary layer could be induced when the SST and SA models are combined with the DDES model.



(a) SADDES and $l=2e-4$ (b) RKEDDES and $l=2e-4$ (c) SSTDDDES and $l=2e-4$

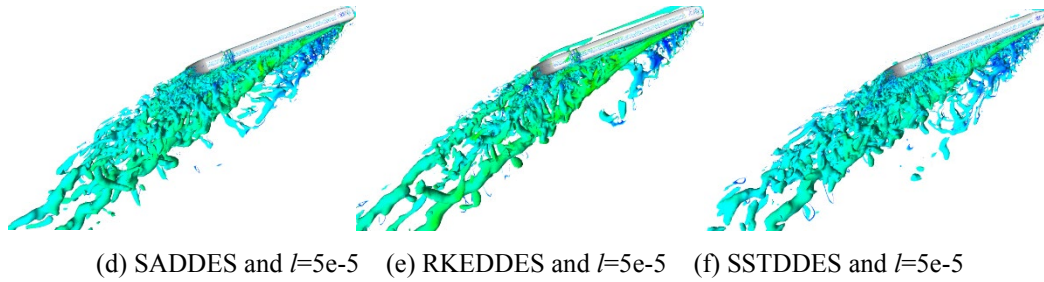


Figure 5: The iso-surfaces of the instantaneous second invariant of the time-averaged velocity gradient at different levels

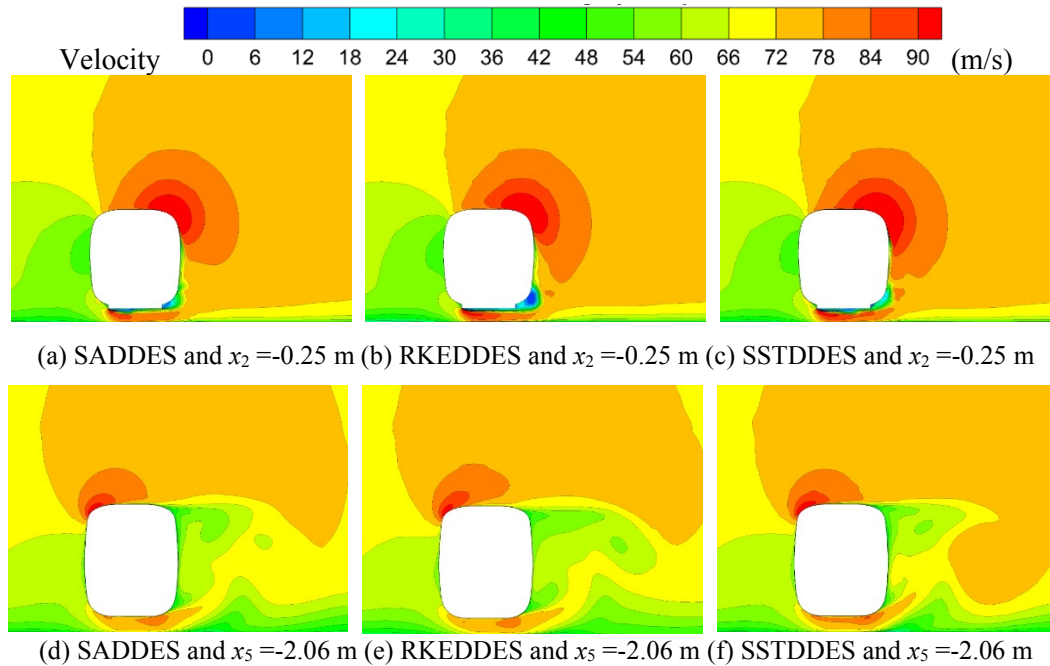


Figure 6: Velocity distribution around the train at different loops

Fig. 6 shows the velocity distribution of two typical cross-sections of the train. The two typical cross-sections are $x_2=-0.25$ m and $x_5=-2.06$ m, respectively. The former cross-section is located in the streamlined part of the body and the latter one is located in the rear of the body. It can be observed that two different cross-sections have different velocity distribution laws. At the cross-section $x_2=-0.25$ m, the region with a high speed is located near the leeward face, the gap between the bottom of the vehicle and the ground. The region with a low speed is mainly located at the corner of the bottom and the lower part of the leeward face due to the shedding vortex. At the cross-section $x_5=-2.06$ m, the region with a high speed is located at the corner of the roof and the windward face, the gap between the train body and ground, and the region with a small speed is mainly located in the area close to the ground and the leeward face of the vehicle body.

The velocity distribution obtained using three different approaches is basically the same.

However, there are specific differences. At the cross-section $x_2 = -0.25$ m, the velocity distribution at the corner of the roof and the leeward face is different. The velocity obtained using the SSTDES is larger, corresponding to the difference in the maximum negative pressure shown in Fig. 3(b). The velocity distribution underneath the train body is also different. Such difference corresponds to the difference in the pressure on the bottom shown in Fig. 3(b). The vortices at the corner of the train bottom and the leeward face obtained by three approaches are different in size, and the vortex obtained by the RKEDDES has formed and gradually separated from the train body. At the cross-section $x_5 = -2.06$ m, the significant difference in the velocity distribution is located underneath the vehicle body. The SSTDES gives the largest velocity among all approaches, and such difference makes the difference in the pressure on the bottom of the vehicle body shown in Fig. 3(e). There are also some differences in the vortex distribution in the wake flow.

4.4 Aerodynamic forces and instantaneous pressure

The aerodynamic forces exerted on the train are due to the relative motion between the train and air. The aerodynamic drag, side and lift forces are discussed in the following.

Fig. 7 shows the time-varying signals of the aerodynamic forces and the corresponding frequency characteristics. According to the coordinate system in Fig. 1, the side force is leeward, and the lift force is downward. In general, the forces vary around their mean values with a considerable magnitude. There are certain differences in forces obtained by different approaches.

For the drag force, the SSTDES predicts a relatively smaller magnitude of the drag force. Both RKEDDES and SADDDES give close mean values for the drag force. The mean value of the drag force for SSTDES is -33.02 N, which is less nearly 35% than those for the RKEDDES and SADDDES. The primary frequencies of the drag forces are less than 100 Hz. The peak frequencies of the drag forces for the RKEDDES, SADDDES and SSTDES are about 29, 32 and 66 Hz, respectively.

For the side force, three approaches predict different mean values. The mean value of the side forces for the RKEDDES is the largest, and that for the SSTDES is the smallest. The mean values of the side forces for the RKEDDES, SADDDES and SSTDES are about 1109.92, 1158.61 and 1188.56 N, respectively. The primary frequencies of the side forces are mainly in the range of 0 Hz to 80 Hz. Both SSTDES and SADDDES give a close primary frequency of the side force, and the peak frequency is about 18.70 Hz, whereas the peak frequency of the side force for the RKEDDES is 13.62 Hz.

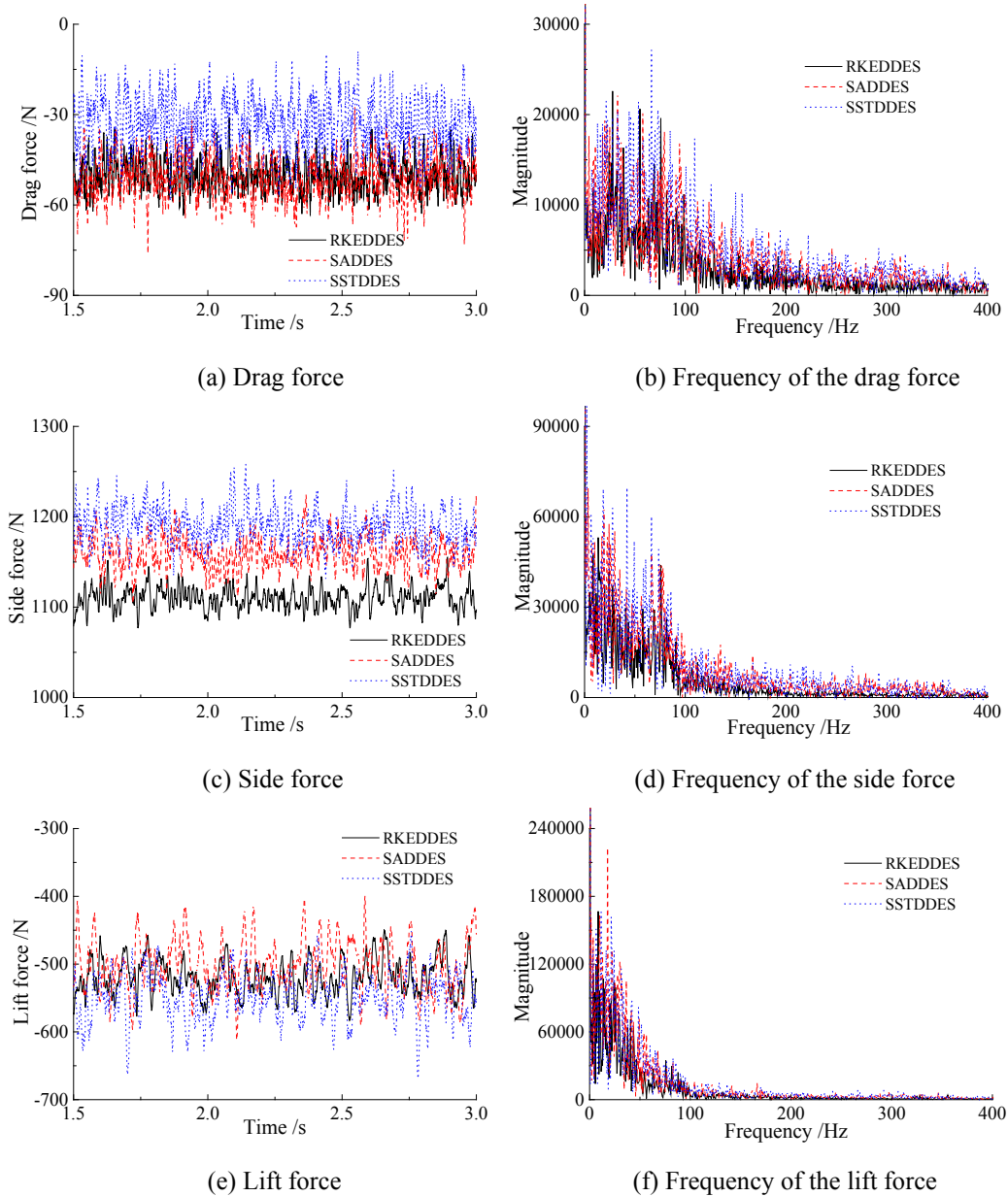


Figure 7: The time-varying signals of the aerodynamic forces and the corresponding frequency characteristics

For the lift force, the SSTDDDES predicts a relatively smaller magnitude of the lift force. The mean values of the lift forces for the RKEDDES, SADDDES and SSTDDDES are about -522.11, -503.23 and -548.75 N, respectively. The primary frequencies of the lift forces are mainly in the range of 0 Hz to 50 Hz. The peak frequencies of the drag forces for the RKEDDES, SADDDES and SSTDDDES are about 8.52, 18.25 and 11.47 Hz, respectively.

As the aerodynamic forces are integrated by the surface pressure, the pressure variations have a significant effect on the variations of the aerodynamics forces. Fig. 8 shows the time-varying signals of the instantaneous pressure on 12 taps at the cross-section $x_4=-1.57$ m. On the roof, the taps near the leeward face predict a larger variation in the pressure than those near the windward face. On the leeward face, the pressure on all taps has a significant variation and the taps close to the bottom surface show a larger variation. This is because the gap that exists between the train body and the ground makes the flow faster. On the bottom face, there are certain variations in pressure due to the narrow gap between the train body and ground. The variation in pressure is related to the flow fluctuation, such as flow separation. On the windward face, there are small variations of the pressure for the taps, especially for the taps in the middle of the windward face.

It can be observed that taps p9, p10 and p3 predict positive pressure all of the time, whereas almost other taps give negative pressure. The taps on the leeward face have the largest root mean square (RMS) among all faces, and the taps on the windward face have the smallest RMS.

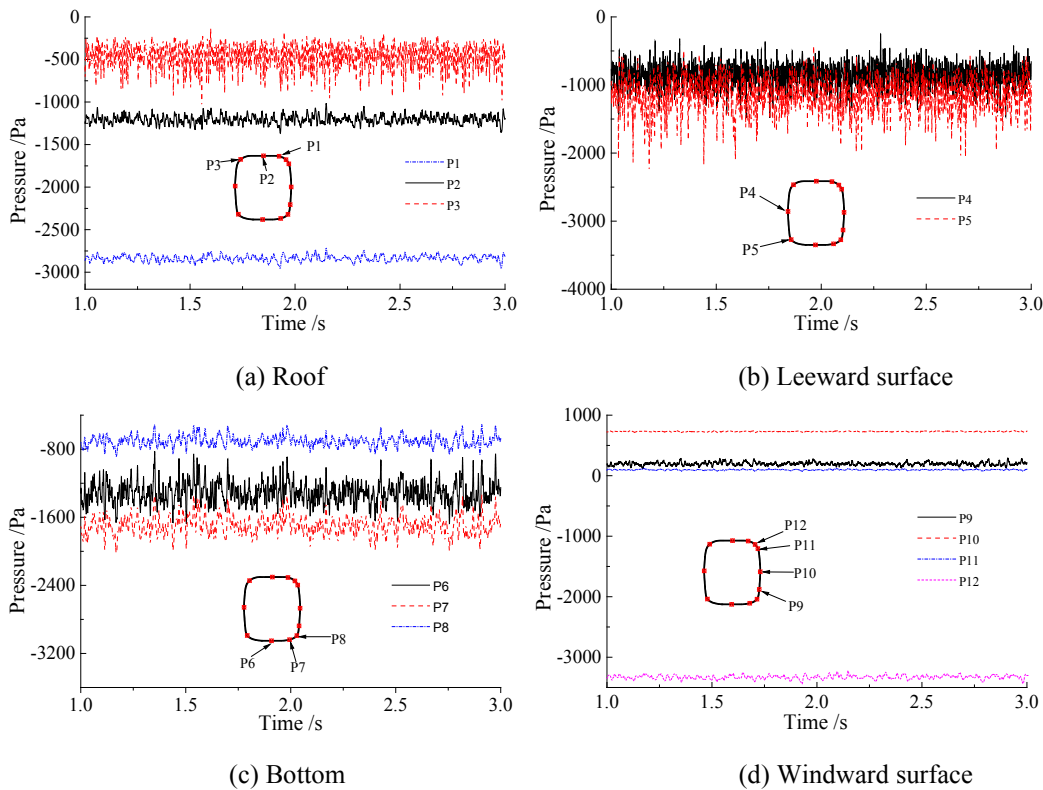


Figure 8: The time-varying signals of the instantaneous pressure at the cross-section $x_4=-1.57$ m

For every time step, it takes about 57.6 seconds for the SADDDES. 71.4 seconds and 72.9 seconds are taken for the KEDDES and SSTDDDES, respectively. The calculation

platform has 48 cores. The SADDES performs a faster calculation compared to the others due to the one -equation SA model.

5 Conclusion

In this work, simulations of the train in crosswinds are conducted using the DDES models based on different RANS models. Furthermore, the effect of RANS models on aerodynamic characteristics is studied. Firstly, the DDES based on the three typical RANS models can give relatively accurate predictions of pressure coefficient on almost all surfaces. The SSTDES predicts more accurate results compared to those obtained using the other DDES models. Secondly, there are certain differences in the small vortices obtained using different RANS models. The RKEDES predicts fewer vortices in the wake flow than the SADDES and SSTDES do. The vortex shells obtained using the SADDES are quite similar to those for the SSTDES. Finally, the variation in the side force is mainly due to the variations in pressure on the leeward face, and the variations in pressure on both the roof and bottom near the leeward face result in the variation in the lift force.

Acknowledgement: This project was supported in part by the National Natural Science Foundation of China (No. 51605397), Sichuan Science and Technology Program (No. 2019YJ0227), China Postdoctoral Science Foundation (No. 2019M663550) and Self-determined Project of State Key Laboratory of Traction Power (2019TPL_T02).

Conflicts of Interest: The authors declare that they have no conflicts of interest to report regarding the present study.

References

- Baker, C. J.** (2019): A review of train aerodynamics: Part 1-Fundamentals. *Aeronautical Journal*, vol. 118, no. 1201, pp. 201-228.
- Bangga, G.; Weihing, P.; Lutz, T.; Krämer, E.** (2017): Effect of computational grid on accurate prediction of a wind turbine rotor using delayed detached-eddy simulations. *Journal of Mechanical Science and Technology*, vol. 31, no. 5, pp. 2359-2364.
- Chen, J. W.; Gao, G. J.** (2016): Detached-eddy simulation of flow around high-speed train on a bridge under cross winds. *Journal of Central South University*, vol. 23, no. 10, pp. 2735-2746.
- Chen, X.; Li, M.** (2019): Delayed detached eddy simulation of subcritical flow past generic side mirror. *Journal of Shanghai Jiaotong University (Science)*, vol. 24, no. 1, pp. 107-112.
- Flynn, D.; Hemida, H.; Soper, D.; Baker, C.** (2014): Detached-eddy simulation of the slipstream of an operational freight train. *Journal of Wind Engineering and Industrial Aerodynamics*, vol. 132, pp. 1-12.
- Guo, Z.; Liu, T.; Yu, M.; Chen, Z.; Li, W. et al.** (2019): Numerical study for the aerodynamic performance of double unit train under crosswind. *Journal of Wind Engineering & Industrial Aerodynamics*, vol. 191, pp. 203-214.

Hedges, L. S.; Travin, A. K.; Spalart, P. R. (2002): Detached-eddy simulations over a simplified landing gear. *Journal of Fluids Engineering*, vol. 124, no. 2, pp. 413-423.

Hemida, H.; Krajnović, S. (2009): Exploring flow structures around a simplified ICE2 train subjected to a 30° side wind using LES. *Engineering Applications of Computational Fluid Mechanics*, vol. 3, pp. 28-41.

Hemida, H.; Krajnovic, S. (2009): Transient simulation of the aerodynamic response of a double-deck bus in gusty winds. *Journal of Fluids Engineering*, vol. 131, no. 3, 031101.

Li, T.; Hemida, H.; Zhang, J. Y.; Rashidi, M.; Flynn, D. (2018): Comparisons of shear stress transport and detached eddy simulations of the flow around trains. *Journal of Fluids Engineering*, vol. 140, no. 11, pp. 1108-1112.

Li, T.; Qin, D.; Zhang J. Y. (2019): Effect of RANS turbulence model on aerodynamic behavior of trains in crosswind. *Chinese Journal of Mechanical Engineering*, vol. 32, pp. 85.

Li, T.; Zhang, J. Y.; Rashidi, M. M.; Yu, M. G. (2019): On the Reynolds-averaged Navier-Stokes modelling of the flow around a simplified train in crosswinds. *Journal of Applied Fluid Mechanics*, vol. 12, no. 2, pp. 551-563.

Maleki, S.; Burton, D.; Thompson, M. C. (2017): Assessment of various turbulence models (ELES, SAS, URANS and RANS) for predicting the aerodynamics of freight train container wagons. *Journal of Wind Engineering and Industrial Aerodynamics*, vol. 170, pp. 68-80.

Menter, F. R. (1994): Two-equation eddy-viscosity turbulence models for engineering applications, *AIAA Journal*, vol. 32, no. 8, pp. 1598-1605.

Menter, F. R.; Kuntz, M.; Langtry, R. (2003): Ten years of industrial experience with the SST turbulence model. *Turbulence, Heat and Mass Transfer*, vol. 4, pp. 624 - 632.

Morden, J. A.; Hemida, H.; Baker, C. J. (2015): Comparison of RANS and detached eddy simulation results to wind-tunnel data for the surface pressures upon a class 43 high-speed train. *Journal of Fluids Engineering*, vol. 137, no. 4, pp. 1108-1109.

Niu, J. Q.; Wang, Y. M.; Zhang, L.; Yuan, Y. P. (2018): Numerical analysis of aerodynamic characteristics of high-speed train with different train nose lengths. *International Journal of Heat and Mass Transfer*, vol. 127, pp. 188-199.

Shur, M.; Spalart, P. R.; Strelets, M.; Travin, A. (1999): Detached-eddy simulation of an airfoil at high angle of attack. *Engineering Turbulence Modelling & Experiments*, vol. 4, pp. 669-678.

Tian, C.; Lu, Y. J. (2013): Turbulence models of separated flow in shock wave thrust vector nozzle. *Engineering Applications of Computational Fluid Mechanics*, vol. 7, no. 2, pp. 182-192.

Vatsa, V. N.; Lockard, D. P.; Spalart, P. R. (2017): Grid sensitivity of SA-based Delayed-Detached-Eddy-Simulation model for blunt-body flows. *AIAA Journal*, vol. 55, no. 8, pp. 1-7.

Walters, D.; Cokljat, D. (2008): A three-equation eddy-viscosity model for Reynolds-Averaged Navier-Stokes simulations of transitional flow. *Journal of Fluids Engineering*, vol. 130, no. 12, pp. 320-327.

Wang, S.; Bell, J. R.; Burton, D.; Herbst, A. H.; Mark, J. S. (2017): The performance of different turbulence models (URANS, SAS and DES) for predicting high-speed train slipstream. *Journal of Wind Engineering & Industrial Aerodynamics*, vol. 165, no. 1, pp. 46-57.

Wilson, R. V.; Stern, F.; Coleman, H. W. (2001): Comprehensive approach to verification and validation of CFD simulations-Part 2: application for RANS simulation of a Cargo/Container Ship. *Journal of Fluids Engineering*, vol. 123, no. 4, pp. 803-810.

Xia, C.; Wang, H. F.; Shan, X. Z.; Yang, Z. G.; Li, Q. L. (2017): Effects of ground configurations on the slipstream and near wake of a high-speed train. *Journal of Wind Engineering & Industrial Aerodynamics*, vol. 168, pp. 177-189.

Yu, M. G.; Jiang, R. C.; Zhang, Q.; Zhang, J. Y. (2019): Crosswind stability evaluation of high-speed train using different wind models. *Chinese Journal of Mechanical Engineering*, vol. 32, pp. 40.